khanika i Teknicheskoi Fiziki, No. 5, 1963; trans. (DDC AD 614 773), pp. 193–202.

[10] Friedman, R. et al., "Deflagration of Ammonium Perchlorate," *Sixth Symposium (International) on Combustion*, Reinhold, New York, 1957, pp. 612–618.

[11] Levy, J. B. and Friedman, R., "Further Studies of Pure Ammonium Perchlorate Deflagration," *Eighth Symposium (International) on Combustion*, Williams and Wilkins, Baltimore, 1962, pp. 663–672.

[12] Irwin, O. R., Salzman, P. K., and Anderson, W. H., "Deflagration Characteristics of Ammonium Perchlorate at High Pressures," *Ninth Symposium (International) on Combustion*, Academic Press, New York, 1963, pp. 358–364.

[13] Watt, D. M., Jr. and Petersen, E. E., "Deflagration and Deflagration Limits of Single Crystals of Ammonium Perchlorate," AF-AFOSR 959-65, Dec. 1968, Univ. of California, Berkeley, Calif.

[14] Hightower, J. D., Price, E. W., and Zurn, D. E., "Continuing Studies of the Combustion of Ammonium Perchlorate," in *4th Combustion Conference*, ICRPG, Ed. Chemical Propulsion Information Agency, Silver Spring, Md., CPIA Publ. 162, Vol. 1, Dec. 1967, pp. 527–534.

[15] Beckstead, M. W. and Hightower, J. D., "Surface Temperature of Deflagrating Ammonium Perchlorate Crystals," *AIAA Journal*, Vol. 5, No. 10, Oct. 1967, pp. 1785–1790.

[16] Hightower, J. D. and Price, E. W., "Experimental Studies Relating to the Combustion Mechanism of Composite Propellants," *Astronautica Acta*, Vol. 14, No. 1, Nov. 1968, pp. 11–21.

[17] Bobolev, V. K. et al. "The Temperature Distribution in Ammonium Perchlorate When Burning," *Doklady Akademii Nauk SSSR*, Vol. 151, No. 3, 1963, pp. 604–607; trans(AD 434110).

[18] Wenograd, J. and Shinnar, R., "Combustion of Ammonium Perchlorate—Some Negative Conclusions," *AIAA Journal*, Vol. 6, No. 5, May 1968, pp. 964–966.

MAY 1970 AIAA JOURNAL VOL. 8, NO. 5

Further Investigations on Low-Density Hall Accelerators

R. Koehne,* F. Lindner,* K. R. Schreitmueller,† H. G. Wichmann,‡ and E. Zeyfang*
Deutsche Forschungs- und Versuchsanstalt fuer Luft-und Raumfahrt,
Institut fuer Energiewandlung und Elektrische Antriebe, Stuttgart, Germany

Based on theoretical considerations, the dependence of the thruster efficiency on the magnetic field and on the length of the accelerator channel has been calculated. To reduce the anomalous electron back-flow, an external ion source should be used which produces a homogeneous ion beam. This can be obtained by an annular plasma source with a slit hollow cathode. Experiments have been carried out on two different accelerator types. The plasma properties in the exhausted beam have been measured using probes and spectroscopical methods. The ion velocity distribution has been measured by a retarding potential method. For the determination of the thrust a pendulum has been used. Further experiments have been done on ion sources.

Nomenclature

Ag = weighted transition
B = magnetic field
E = electric field
J = relative line intensity
Q = cross-section for collisions
T = temperature
U = accelerator voltage
W = excitation energy
j = current density
k = Boltzmann constant
l = accelerator length
m = mass
n = particle density
p = pressure
q = electric charge
r = radial coordinate
t = time
v = velocity
z = axial coordinate
η = efficiency
λ = wave length
σ = electric conductivity
φ = azimuthal coordinate
ω = angular velocity

Subscripts

c = cyclotron
e = electron
i = ion
o = neutral

Presented as Paper 69-281 at the AIAA 7th Electric Propulsion Conference, Williamsburg, Va., March 3–5, 1969; submitted March 3, 1969; revision received September 15, 1969. The authors wish to thank E. Knoernschild for his interest in this research program.

* Diplom-Physiker.
† Doktor-Ingenieur.
‡ Doktor rerum naturalium.

1. Introduction

In the near future, several missions into the near space, orbit-to-orbit transfer, and mapping of the Van Allen Belt, etc., can be realized by using electric thrusters. The electric power requirements for these missions are in the range of 1–20 kw. Typical thruster data are mass flow rates $\sim 10^{-6}$ kg/sec, exhaust velocities between 20 to 50 km/s, thrusts between 10^{-2} to 2.10^{-1} N.

Of all electric thrusters the ion thrusters have reached the highest status of development up to date. Their main field of application, however, appears to be missions, where exhaust velocities between 50 km/sec and 100 km/sec are required. Good results have also been obtained with MPD-arcjets. The practical range of electric power input, however, is in general beyond that needed for the missions mentioned previously. Hence, there is a gap in the spectrum of thrusters available up to date which can be closed by Hall ion-thrusters. The power requirement of these thrusters is between 0.5 to 5 kw, the velocity range 20–50 km/sec. The principle of the Hall ion-thrusters is based on the acceleration of ions as in

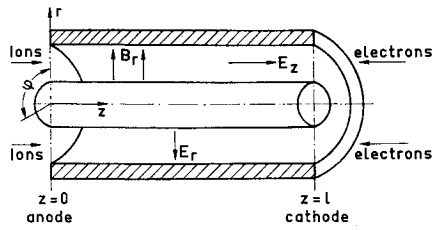

Fig. 1 Schematic drawing of the accelerator with notations.

the case of ion engines. However, the limitation of the current density in ion motors, caused by space charge effects, is overcome by neutralizing the space charge in the accelerator region. This is done using a magnetic field, which is perpendicular to the electric accelerating field, and permits the acceleration of the ions within a neutral plasma. Therefore, an Hall ion-accelerator can be operated with essentially higher current densities. Furthermore, the geometric dimensions of this type can be reduced which leads to an increase of the ratio exhaust power to thruster weight.

First studies on Hall accelerators date back to the early sixties.[1-9] The authors used magnetic cusp fields or magnetic pot core geometry. The working gas was argon or cesium. Based on the results of some of these investigations we started our research program in 1965. Our first studies were reported elsewhere.[10,11] In the following, further investigations are presented. The aim of these studies was to get a better knowledge of the plasma processes, to improve the technological status, and to develop an advanced thruster type.

2. Theory

At low densities the mean free path of a particle is of the order of magnitude of the accelerator length. Therefore, the motion of a single particle may be representative for the whole plasma motion. With a cylindrical system of coordinates r, φ, z (Fig. 1) and the fields

$$\mathbf{E} = (E_r, 0, E_z)(E_r \ll E_z) \text{ and } \mathbf{B} = (B_r, 0, 0)$$

the velocities of the particle in φ resp. z direction result in

$$v_\varphi = \left(v_{\varphi 0} - \frac{E_z}{B_r}\right)\cos\omega_c t + \frac{E_z}{B_r} + v_{z0}\sin\omega_c t \tag{1a}$$

$$v_z = \left(\frac{E_z}{B_r} - v_{\varphi 0}\right)\sin\omega_c t + v_{z0}\cos\omega_c t$$

with (1b)

$$\omega_c = \frac{qB_r}{m} \text{ and } v_0 = v(t = 0)$$

The radial electric field E_r prevents an outwardly directed drift due to centrifugal and magnetic mirror forces. Averaging all initial velocities v_o, the azimuthal velocity of the particle is

$$\bar{v}_\varphi = +(E_z/B_r)(1 - \cos\omega_c t) \tag{2a}$$

hence, the motion is cycloidic.

In z direction the particle is oscillating between $z = 0$ and $z = 2r_c$, where r_c is given by

$$r_c = mE_z/qBr^2$$

Because of the different cyclotron radius of the ions and electrons the ions are accelerated by the electric field and barely influenced by the magnetic field whereas the electrons are captured by the magnetic field.

However, if there exists an additional axial component of the magnetic field

$$\mathbf{B} = (B_r, 0, B_z)(B_z \ll B_r)$$

the axial motion of the particle is

$$v_z = v_z(B_z = 0) + \frac{q}{m} E_z \frac{B_z^2}{B_r^2 + B_z^2}\cdot t \tag{2b}$$

Now, an axial motion of the electrons is possible. Because of the high mobility of the electrons even very small axial components of the magnetic field ($\approx 1 \ldots 3\%$) cause a high electron back-flow and corresponding high losses. Thus, an effective acceleration of the ions is only possible in a pot core magnetic system, but not in cusp field accelerators.

However, if collisions between electrons and ions cannot be neglected, even in the case of vanishing axial magnetic fields an electron back-flow takes place. This classical electron diffusion generates an axial electron current density

$$j_e = \frac{m_e E_z n_e n_i Q_{ei}}{B_r^2}\cdot\left(\frac{3kT_e}{m_e} + \frac{2E_z^2}{B_r^2}\right)^{1/2} \tag{3}$$

As

$$\frac{3kT_e}{m} \gg 2\frac{E_z^2}{B_r^2}$$

it follows

$$j_e \sim \frac{E_z}{B_r^2}$$

Due to plasma effects there are induced electric and magnetic fields within the accelerator region which distort the applied fields. If, for example, the carrier density is not homogeneous in azimuthal direction, the electron cloud, drifting in φ direction, will be separated from the ion cloud. Thus, an azimuthal electric field E_φ is set up which causes an electron drift in axial direction. The current density of this anomalous electron diffusion is

$$j_e = n_e e(E\varphi/B_r) \sim 1/B_r \tag{4}$$

In some previous publications[7,8,12] the problem of the anomalous electron diffusion has been discussed and several suggestions to avoid the onset of instabilities were given. To obtain an effective acceleration it is therefore necessary to operate the thruster under conditions where no instabilities occur.

The following considerations are based on these conditions. Furthermore, ionization, thermalization, or recombination effects inside the accelerator channel are neglected.

However, even in this case space charge neutralization is not established automatically. For complete space charge neutralization (this means E_z = const) the current continuity equation leads to the following expression for the magnetic field:

$$B_r(z) = B_r(0)/(1 + 2eUz/lm_i v_{io}^2)^{1/2} \tag{5}$$

Hence, the magnetic field strength is inversely proportional to the ion velocity. The assumption of a constant magnetic field leads to an expression for the electric field, given by

$$E_z(z) = (m_i v_{io}^2 \gamma^{2z/l} \ln\gamma/ql) \tag{6}$$

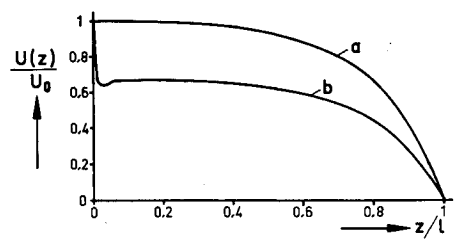

Fig. 2 Potential shape within the accelerator a) with external ionization; b) with internal ionization.

where

$$\gamma = (1 + 2eU/m_i v_{io}^2)^{1/2} = v_i(l)/v_i(0) \qquad (7)$$

This means that a complete space charge neutralization can only be obtained applying a radial magnetic field, which decreases in the z direction. The potential shape corresponding to Eq. (6) is shown in Fig. 2a. The high cathode fall consequently results not from the carrier production near the cathode, but from the electron diffusion across the magnetic field. The anode fall disappears.

However, with internal ion production, the anode fall reaches values well beyond the ionization potential, as shown in Fig. 2b. With low electron back-flow, each electron entering the anode fall region generates there one or several ions. While the ions leave the anode region, the likewise produced electrons are retained by the magnetic field. The negative spacecharge generates the high electric field in the fall region, which maintains the current continuity in front of the anode. Because of the high electric field strength, the electrons obtain rather high velocities, which may falsify measurements with Langmuir probes.

Equations (5) and (6) describe two different accelerator types with external ion production. The E-type-accelerator (E = const) has less wall losses and a lower ion deflection by the magnetic field than the B-type-accelerator (B = const). Basically E-type-accelerators promise a higher efficiency. However, as the difference in efficiency between both accelerators is rather small, we use the B-type-accelerator, because of its simpler design. The following discussion on optimization problems is therefore based on this type.

Two factors are influencing the acceleration efficiency:

1) the ratio of ion current to total current,

$$\eta_{ei} = j_i/(j_i + j_e) \qquad (8)$$

2) the ratio of axial ion velocity to total ion velocity at the accelerator exit,

$$\eta_{is} = v_z(v_z^2 + v_\varphi^2)^{-1/2} \qquad (9)$$

The over-all efficiency $\eta = \eta_{ie}\,\eta_{is}$ increases with decreasing accelerator length if the product of B and l remains constant. Short accelerators with correspondingly high magnetic fields result in good efficiencies. With given accelerator length, there exists an optimal ratio $\bar{E}/B$ ($\bar{E} = U/l$). Higher values result in a large electron back-flow, with lower values the ions are too much deflected by the magnetic field. The optimum depends on the choice of the gas, on the carrier density and on the exit velocity. Generally, the design of a Hall ion-accelerator is based on the magnetic field energy rather than on the accelerator length. Assuming a constant magnetic gap area, the efficiency increases with decreasing accelerator length and increasing magnetic energy. In Fig. 3 the optimal magnetic energy and the corresponding efficiency are plotted vs the accelerator length.

Hereby the magnetic energy is characterized by the integral

$$M = \int_{-\infty}^{+\infty} B^2 dZ$$

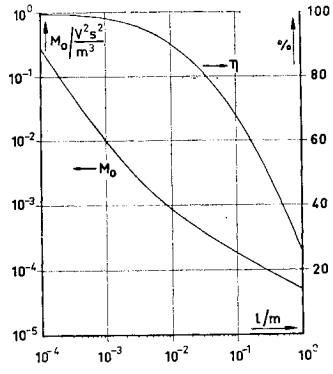

Fig. 3 Optimal magnetic energy M_0 and corresponding efficiency vs accelerator length. Argon, exit velocity 20 km/sec, initial ion density 10^{20} m^{-3}.

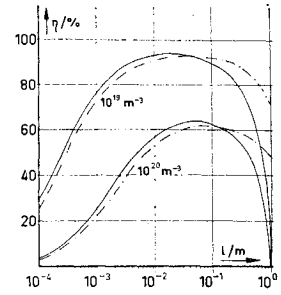

Fig. 4 Efficiency vs accelerator length. Magnetic energy coefficient. $M_0 = 10^{-4}$ V^{2}s^2/m^3.

From these calculations it follows that in the case of small accelerator lengths, even a considerable rise of the magnetic field energy increases the efficiency only very little. This is due to the fact that the ratio of the energy, stored in the stray field, to the useful magnetic energy becomes greater for small accelerator lengths. For a given magnetic energy there exists an optimal accelerator length, for which the magnetic field is strong enough to prevent high electron backflow, but for which the magnetic stray fields are not yet so important. Figure 4 shows the efficiency vs accelerator length for given magnetic energy and for two carrier densities and exit velocities in the case of argon as the fluid.

3. Experiments

Experiments have been carried out on two different accelerator types.

1) HIT III (Hall Ion-Thruster III). Ion production by volume ionization in the accelerator channel itself; variable magnetic field produced by an electro-magnet; variable channel length up to 10 cm.

2) HIT IV (Hall Ion-Thruster IV). External ion production; magnetic field produced by permanent magnets; short and not variable channel length.

3.1. Measurements on the Type HIT III

3.1.1. Electric measurements

A schematic sketch of the thruster HIT III is shown in Fig. 5. The accelerator was operated with argon. In Fig. 6 the current voltage characteristics are plotted at different magnetic field strengths. The observed minimum is explained by two oppositely directed effects. It is known that the electric field strength in the positive column of a discharge decreases with increasing current density. However, a high-discharge current results in a high-current density in the anode region, and this effect causes an increasing anode fall, which becomes mainly important in the case of non-self-sustained discharges with heated cathodes, because now the anode fall cannot be neglected compared with the cathode fall. An increase of the magnetic field-strength demands higher voltages for the same discharge current. The reason is that with higher magnetic fields the electrons are increasingly restrained in their motion. Corresponding to the physical conditions of our accelerator an

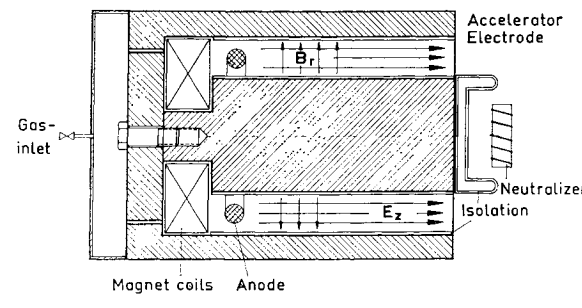

Fig. 5 Cross section of the thruster HIT III.

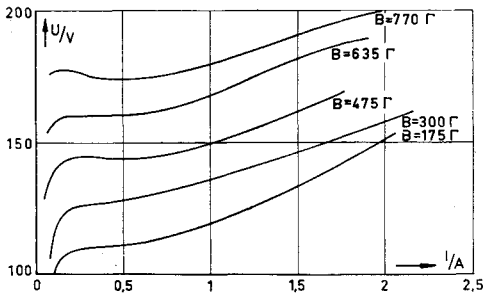

Fig. 6 Current voltage characteristics. Parameter: magnetic field strength.

optimal magnetic field strength of about 300 gauss has been evaluated theoretically. However, as it can be seen in Fig. 6 magnetic field strengths above this value have still a strong influence on the current-voltage characteristics. It seems to be advantageous to choose a higher magnetic field strength, since it reduces the electron back-flow and the losses due to this backflow.

Measurements of the exhausted ion beam have been carried out by a coaxial double probe[13] as well as by a retarding potential method. The double probe consists of a metallic tube and a rod electrode positioned in the axis of the tube, so that the plasma beam can pass the probe nearly unhindered. The probe was used floating in order to prevent a net current from the discharge. An operational condition of the probe is that ion saturation must be reached before electron saturation occurs. This means that the area ratio of the two electrodes should not exceed an upper limit. Furthermore, the free passing ion beam should be negligible with respect to the measured ion beam. The applied voltage should be as low as possible to prevent any production of secondary electrons by ion bombardment, but high enough to operate the probe in the region of ion saturation. In Fig. 7 typical probe measurements are shown. The ion current is plotted versus the radial magnetic field strength in the acceleration channel, parameter is the discharge current in the accelerator.

The maximum of ion current at a magnetic field strength of 300 gauss agrees well with our theoretical calculations. However, the real values for the ion current are certainly higher than the measured values. As mentioned previously, a part of the ion beam will pass through the probe. Besides the exhausted ion beam recombines partly with the emitted electrons before reaching the probe. This can be shown by varying the number of the emitted electrons as well as by shifting the probe in the beam axis.

The arrangement for measuring the ion current with the retarding potential method is presented in Fig. 8. A closed wire cage was put on the accelerator exit and connected over a variable load with the neutralizer. Between grid and neutralizer an insulated plate was attached to prevent too much electrons from coming to the gate. By the magnetic stray-field these electrons were furthermore hindered to reach the grid.

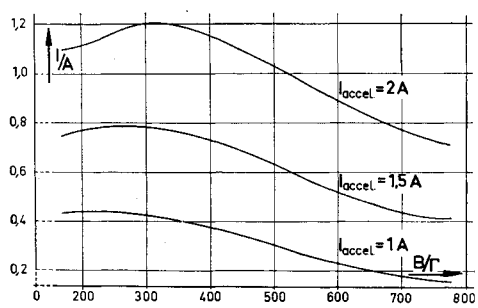

Fig. 7 Ion current in the exhausted beam vs magnetic field. Parameter: $I_{accel.}$.

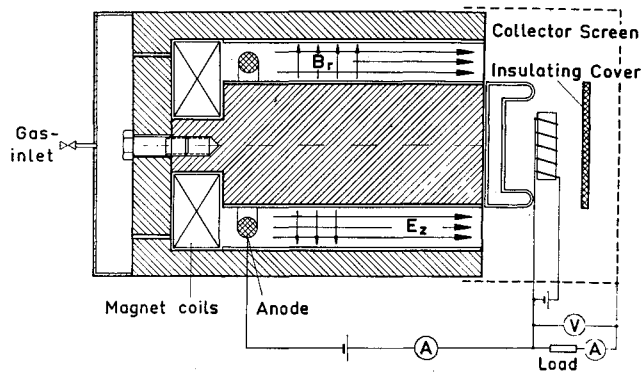

Fig. 8 Retarding potential method arrangement.

The retarding potential for the ions in the beam is created by the ions themselves. It depends on their velocity and on the value of the variable load. If the resistance is varied from $R = 0$ up to $R = \infty$ one obtains the dependence of the exhausted ion beam on the retarding potential U which is proportional to the square root of the ion velocity (Fig. 9a). The ion current measured at $R = 0$ ohms, corresponds rather well with the measurements using the coaxial double probe. Also in this case there are errors due to recombinations and free passing ions. Furthermore, it cannot be excluded, that electrons reach the grid after passing the magnetic stray field.

Measuring the ion current in dependence of the retarding potential a velocity distribution of the accelerated ions can be derived (Fig. 9b). It can be concluded from the distinct peak in the velocity distribution that nearly all ions are within a very narrow velocity range.

Furthermore, the retarding potential method serves for the determination of the electric efficiency of the whole setup. However, the maximum output power of the exhausted beam is not obtained for one half of the open circuit voltage of the ion detector as it is usual for linear current-voltage conditions. The reason is seen from the measured velocity distribution. Here the maximum power is obtained for voltages near the open circuit voltage. The total efficiency of the set-up is the product of accelerator and detector efficiency. The measured value was 24%. Assuming the same efficiency for both an electric efficiency of the accelerator of 49% may be derivated. This value corresponds with other measurements.

3.1.2. Spectroscopical measurements

The spectroscopical measurements have been carried out using a Hilger and Watts Medium Quartz Spectrograph. With this apparatus the electron temperature and the electri-

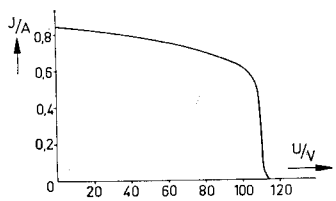

Fig. 9a Exhausted ion beam vs retarding potential.

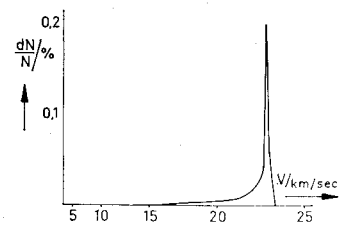

Fig. 9b Velocity distribution in the exhausted ion beam.

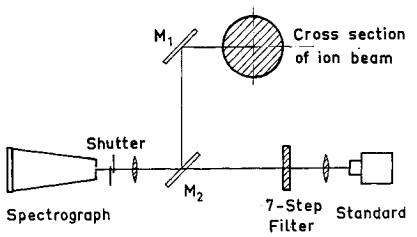

Fig. 10 Optical measuring arrangement.

cal conductivity could be determined. The optical arrangement is presented in Fig. 10.

The electron temperature was determined from the relative intensity ratio of two argon lines of subsequent ionization stages. Assuming at first a Boltzmann distribution for the population of the various levels, one gets

$$\frac{J_{II}}{J_I} = \frac{(Ag/\lambda)_{II}}{(Ag/\lambda)_I} \frac{n_i}{n_o} \exp\frac{-W_n^{(i)} + W_n^{(o)}}{kT_e} \qquad (10)$$

Ag is the weighted transition probability, n_i, n_o the total density of ions and atoms, respectively, and W_n the excitation energies. If LTE exists, n_i/n_o may be replaced by the Saha equation $S(n_e, T_e)$ where the electron density n_e—unless measured directly—may be estimated approximately by the gas equation. This is sufficient in most cases;

$$n_e = p/kT_e(F/G + F + 1) \qquad (11)$$

where p is gas pressure, $F = T_o/T_e$, $G = n_e/n_o$. Besides, it is assumed that the electron density is equal to the ion density and the ion temperature T_i is equal to the temperature of the neutral particles T_o. It follows from Eq. (11) that there is always an upper limit for $n_e{:}n_e < p/kT_e$.

Whether LTE exists depends mainly on the electron density and can be estimated.[14] For very small electron densities n_i/n_o will be substituted by the Corona formula. There are again criteria for the validity of this formula.[15]

If the previously assumed Boltzmann distribution is not valid the density ratio has to be multiplied by a factor larger than one, because in nonthermal plasmas the ground level is generally overpopulated compared with the Boltzmann distribution; but this fact has been neglected for the first determination of temperature.

However, one has to realize and estimate whether a Maxwellian distribution of the free electrons exists[16] and whether a diffusion of neutral particles into the hot plasma takes place or not. If, for instance, the diffusion has not been considered, the measured temperatures may differ from the real temperatures by an order of magnitude.[17] The electric conductivity was calculated from the formula of Spitzer. Because of quasi-neutrality and an ionization degree larger 10% one gets numerically

$$\sigma = \frac{408}{T_e^{1/2}\, Q_{ei}} \frac{1}{9\cdot 10^9} (\Omega m)^{-1} \qquad (12)$$

with

$$Q_{ei} = \frac{2.73\cdot 10^{-10}}{T_e^2} \ln\frac{(8756\, T_e^{3/2})}{n_e^{1/2}}\, m^2$$

Substituting the upper limit of Eq. (11) into Eq. (10) (operating pressure $p = 6.10^{-2}$ mm Hg) and calculating the temperature assuming at first LTE one obtains a temperature of 25,000°K and n_e smaller than $2.10^{19}/m^3$. However, from the validity criteria for LTE and Corona, respectively, one recognizes that one has to determine the temperature by the Corona formula. Then the maximum electron temperature is

$$T_e = 16{,}000°\mathrm{K} \qquad n_e \lesssim 4.10^{19}/m^3$$

The temperature distribution is plotted in Fig. 11 vs the diameter D of the plasma.

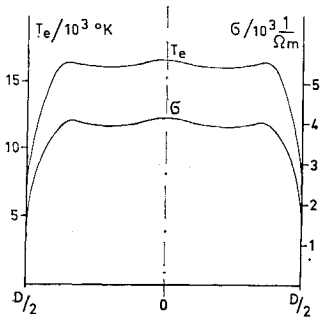

Fig. 11 Radial distribution of temperature and conductivity in the exhausted beam.

From Eq. (13) the electrical conductivity was calculated. Its value is 4000 $1/\Omega m$ and its distribution—also presented in Fig. 11—corresponds virtually to the temperature distribution.

The maximum error in the temperature determination is about ±30%, in the conductivity σ because of σ proportional $T_e^{3/2}$ about ±45%. The electron density may be estimated at a factor 2–3.

3.2. Measurements on the Type HIT IV

A new recently developed accelerator type is shown in Fig. 12. Anode 1 is an annular hollow cathode for an auxiliary discharge burning between anode 1 and anode 2. This discharge is a glow discharge with anomalous cathode fall. So, the cathode area is completely covered by the discharge and the ion production is homogeneous on the periphery. The ions are accelerated by the electric field between anode 1 and the cathode. The magnetic field can be varied up to 0.2 Wb/m^2 according to the number of the employed magnets. The cathode material is thoriated tungsten. The position of the cathode is in a region where no magnetic stray fields exist in order to avoid instabilities originating from the cathode region.

The thrust of this engine was measured with a pendulum. The experiments were carried out with a medium magnetic field of about 0.1 Wb/m^2. At low power levels one gets a thrust to power ratio of about 30–35 mN/kw with an exhaust velocity of some 25–30 km/sec. The ion velocity has been measured using the retarding potential method described in chapter 3.11. Thus a falsification of the measurements due to entrainment of cold gas was prevented. Moreover, the ambient pressure was rather low (3–5 μ Hg). If the power input exceeds 2.5 kw, the thrust is diminishing. This may be explained by an increased electron back-flow due to an enlarged anomalous diffusion. Measurements on instabilities—mainly with Langmuir-probes—are not yet finished.

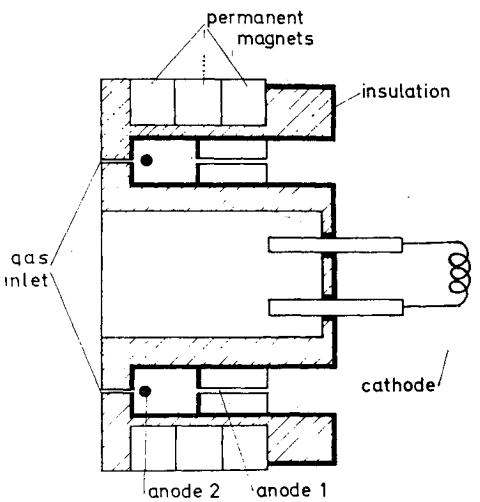

Fig. 12 Cross section of the thruster HIT IV.

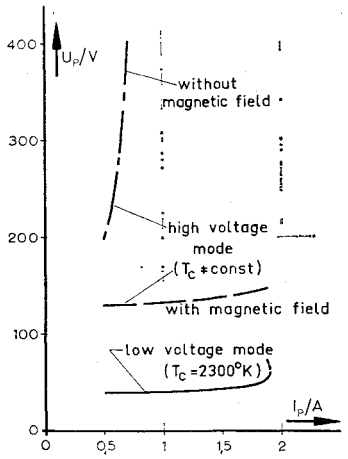

Fig. 13 Current voltage characteristics of a plasma source.

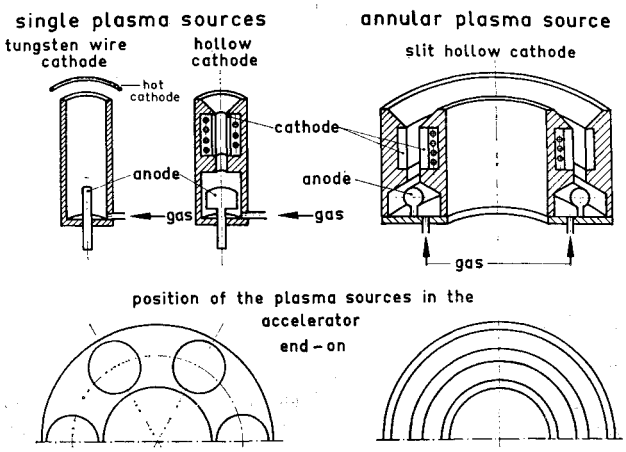

Fig. 15 Cross section of plasma sources.

3.3. Measurements on Plasma Sources

The ionization of the gas (argon) in the plasma sources is obtained using a high-current glow discharge with a heated cathode.[18] The discharge takes place in a ceramic pipe (diam 0.6 cm) between a tungsten anode and a directly heated thoriated tungsten wire as the cathode. Six of these plasma sources are positioned in an annular configuration at the entrance of the accelerator. The mass flow rate through each of the plasma sources is 10^{-6} kg/sec. The gas pressure in the discharge decreases from ca. 1 torr at the entrance to ca. 10^{-1} torr at the exit of the plasma source.

To check the operating conditions of the plasma sources the current-voltage characteristics have been measured. Additional measurements of the exhausted ion current have been carried out on a separated test set-up using a coax double probe.[19]

The current-voltage characteristics are shown in Fig. 13. Depending on the temperature of the heated cathode two different discharge modes can be observed.

a) *Low-voltage mode*: This mode takes place for temperatures of the cathode higher than 2100°K. The shape of the characteristic is approximately horizontal as long as the discharge current is smaller than the saturation current of the hot cathode. For higher discharge currents an increase of the voltage can be observed. In this case the number of electrons emitted from the cathode is too small to sustain the discharge, so that additional electrons must be produced in the discharge region by collisions. This process demands a higher electric field.

Since the plasma sources are positioned at the entrance of the accelerator, there exists a magnetic field in the cathode region of the discharge which could influence the operation conditions. However, it has been observed that in the case of the low-voltage mode this influence is negligible.

From measurements of the ion production it can be concluded that the rate of ionization is rather low (<5%), while the effective ionization energy is high (>1000 ev/ion).

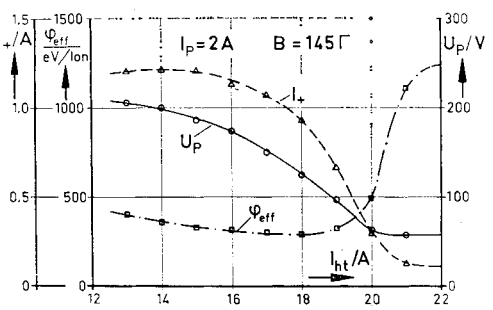

Fig. 14 Discharge voltage, ion current, and effective ionization energy vs cathode heating current.

b) *High-voltage mode*: This mode takes place for temperatures of the cathode below 2000°K. The number of electrons emitted from the cathode is now too small to sustain the low voltage discharge even at small discharge currents. Therefore, the discharge conditions are similar to those of a glow discharge. As the diameter of the discharge pipe and the cross section of the accelerator channel are smaller than the normal cathode dark space, a constricted glow discharge results with very high discharge voltages.

If the magnetic field of the accelerator is switched on, a marked change of the current-voltage characteristic is observed. In this case a transverse magnetic field exists in the cathode region, which results in a decrease in the length of the cathode dark space. According to the similarity laws, this effect is equivalent to an increase of the pressure. This means that the discharge is no more constricted and therefore lower voltages are sufficient. The measured shape of the current-voltage characteristic is approximately horizontal.

In the case of the high-voltage mode the ion production depends considerably on the magnetic field strength in the cathode region and on the temperature of the cathode. For discharge currents of 2 amps an optimal ion production has been obtained at a magnetic field strength of about 150 Γ. Figure 14 represents the applied voltage, the exhausted ion beam, and the effective ionization energy depending on the temperature of the cathode.

With decreasing temperature of the cathode the applied voltage U_P increases from 40 v up to 200 v, the exhausted ion beam varies from 0.1 amps up to a maximum value of 1.2 amps at U_P = 190 v. This value corresponds to an ionization degree of α = 55%. The effective ionization energy has a minimum value of 290 ev/ion for U_P = 125 v. The corresponding ionization degree is α = 43%.

The effective ionization energy has been calculated assuming a heating power of the cathode of 10 watts per amp of emitted electron current. This value can be obtained using oxide cathodes.

The measurements can be explained in the following way: the ionization probability depends on the energy of the electrons. For ionization by electron impact one gets a maximum of the ionization probability (in the case of Argon) for an electron energy of 100 ev to 200 ev. Thus, rather large electric field strengths are necessary. However, high applied voltages result in a large power input which has disadvantages in respect to the ionization energy. Therefore, one has to expect—and the measurements prove it—an optimal value for the applied voltages (see Fig. 14).

Looking forward we intend to develop a new advanced hall ion thruster based on the experiences made on the type HIT IV. In this case the six single plasma sources will be replaced by one annular plasma source with a slit hollow cathode (Fig. 15). The hollow cathode consists of two

coax metal rings, one of these is the indirectly heated oxide cathode. This plasma source has the advantage, that the ion beam entering the accelerator region is homogeneous at the circumference of the channel. This condition is important particularly for short accelerator lengths.

References

[1] Hess, R. V., "Fundamentals of Plasma Interaction with Electric and Magnetic Fields," *Proceedings of the NASA University Conference*, Chicago, Ill., 1962, pp. 313–336.

[2] Sevier, J. R., Hess, R. V., and Brockmann, Ph., "Coaxial Hall Current Accelerator Operation at Forces and Efficiencies Comparable to Conventional Crossed-Field Accelerators," *ARS Journal*, Vol. 32, No. 1, Jan. 1962, pp. 78–80.

[3] Seikel, G. R. and Reshotko, E., "Hall Current Ion Accelerator," *Bulletin of the American Physical Society*, Vol. 7, No. 6, June 1962.

[4] Janes, G. S., Wilson, T., and Dotson, J., "Electrostatic Acceleration of Neutral Plasmas.—Momentum Transfer Through Magnetic Fields," *Proceedings of the III Symposium on Advanced Propulsion Concepts*, Vol. 7, Cincinnati, Ohio, Oct. 1962.

[5] Patrick, R. M. and Powers, W. E., "A Magnetic Annular Arc," Research Rept. 129, May 1962, Avco Everett Research Lab., Everett, Mass.

[6] Cann, G. L., Ziemer, R. W., and Marlotte, G. L., "The Hall Current Plasma Accelerator," AIAA Paper 63-011, 1963, Colorado Springs, Colo.

[7] Lary, E. C., Meyerand, R. G., and Salz, F., "Fluctuations in a Gyro-Dominated Plasma," *Proceedings of the VI Conference on Ionization Phenomena in Gases*, Vol. 2, Paris 1963, pp. 441–449.

[8] Brown, C. O. and Pinsley, E. A., "Further Experimental Investigations of a Cesium Hall-Current Accelerator," *AIAA Journal*, Vol. 3, No. 5, May 1965, pp. 853–859.

[9] Janes, G. S. and Lowder, R. S., "Anomalous Electron Diffusion and Ion Acceleration in a Low-Density Plasma," *The Physics of Fluids*, Vol. 9, No. 6, June 1966, pp. 1115–1123.

[10] Lindner, F. and Wichmann, H. G., "Untersuchungen über die Funktionsweise von Hallstrombeschleunigern," paper presented the DGRR-Symposium Elektrische Raumantriebe, Sonneberg/Harz, Feb. 1966.

[11] Lindner, F. et al., "Investigations on a Low Density Hall Accelerator," paper presented at the 9th Symposium on Engineering Aspects of Magnetohydrodynamics, University of Tenn., April 1968.

[12] Sidney, B. D., Hess, R. V., and Allario, F., "Onset and Suppression of Plasma Instability in Crossed-Field Geometry," *Bulletin of the American Physical Society*, Vol. 13, 1968, p. 839.

[13] Johnson, E. O. and Malter, L., "A Floating Double Probe Method for Measurements in Gas Discharges," *Physical Review*, Vol. 80, No. 1, Oct. 1950, pp. 58–68.

[14] Griem, H. R., *Plasmaspectroscopy*, McGraw-Hill, New York, 1964.

[15] Kolb, A. C. and McWhirter, R. W. P., "Ionization Rates and Power Loss From Θ Pinches," *The Physics of Fluids*, Vol. 7, No. 4, April 1964, pp. 519–531.

[16] Drawin, H. W., "Zur spektroskopischen Temperatur- und Dichtemessung von Plasmen bei Abwesenheit thermodynamischen Gleichgewichts," *Zeitschrift für Physik*, Vol. 172, No. 4, Feb. 1963, pp. 429–452.

[17] Drawin, H. W., Fumelli, M., and Weste, G., "Spectroscopic Investigation of a H and He Plasma in a P.I.G. Discharge," *Zeitschrift für Naturforschung*, Vol. 20a, No. 2, 1965, pp. 184–193.

[18] Schreitmüller, K., "Entwicklung einer Plasmaquelle für Hallbeschleuniger," paper presented at the DGRR-Symposium Elektrische Raumantriebe, Sonneberg/Harz, Feb. 1966.

[19] Zeyfang, E., "Untersuchungen an Plasmaquellen für Hallionenbeschleuniger," DVL-Bericht Nr. 854, Nov. 1968, Deutsche Versuchsanstalt für Luft–und Raumfahrt, Stuttgart, W. Germany.